

UC San Diego

UC San Diego Previously Published Works

Title

An AMPK-caspase-6 axis controls liver damage in nonalcoholic steatohepatitis

Permalink

<https://escholarship.org/uc/item/2h79w48g>

Journal

Science, 367(6478)

ISSN

0036-8075

Authors

Zhao, Peng
Sun, Xiaoli
Chaggan, Cynthia
[et al.](#)

Publication Date

2020-02-07

DOI

10.1126/science.aay0542

Peer reviewed



Published in final edited form as:

Science. 2020 February 07; 367(6478): 652–660. doi:10.1126/science.aay0542.

An AMPK–caspase-6 axis controls liver damage in nonalcoholic steatohepatitis

Peng Zhao^{1,*†}, Xiaoli Sun^{1,†}, Cynthia Chaggan¹, Zhongji Liao¹, Kai in Wong¹, Feng He², Seema Singh³, Rohit Loomba³, Michael Karin², Joseph L. Witztum¹, Alan R. Saltiel^{1,2,*}

¹Department of Medicine, School of Medicine, University of California, San Diego, La Jolla, CA 92093, USA.

²Department of Pharmacology, School of Medicine, University of California, San Diego, La Jolla, CA 92093, USA.

³NAFLD Research Center, Division of Gastroenterology, Department of Medicine, University of California, San Diego, La Jolla, CA 92093, USA.

Abstract

Liver cell death has an essential role in nonalcoholic steatohepatitis (NASH). The activity of the energy sensor adenosine monophosphate (AMP)–activated protein kinase (AMPK) is repressed in NASH. Liver-specific AMPK knockout aggravated liver damage in mouse NASH models. AMPK phosphorylated proapoptotic caspase-6 protein to inhibit its activation, keeping hepatocyte apoptosis in check. Suppression of AMPK activity relieved this inhibition, rendering caspase-6 activated in human and mouse NASH. AMPK activation or caspase-6 inhibition, even after the onset of NASH, improved liver damage and fibrosis. Once phosphorylation was decreased, caspase-6 was activated by caspase-3 or –7. Active caspase-6 cleaved Bid to induce cytochrome c release, generating a feedforward loop that leads to hepatocyte death. Thus, the AMPK–caspase-6 axis regulates liver damage in NASH, implicating AMPK and caspase-6 as therapeutic targets.

Nonalcoholic steatohepatitis (NASH)—characterized by hepatic steatosis, inflammation, and liver damage—has become a leading cause of liver transplant and liver-associated death. Hepatocellular death, characterized by swollen hepatocytes on liver biopsy, is a cardinal feature of NASH (1, 2). In healthy liver, hepatocyte apoptosis has a key role in liver

*Corresponding author. asaltiel@ucsd.edu (A.R.S.); pez021@ucsd.edu (P.Z.).

†These authors contributed equally to this work.

Author contributions: P.Z. conceived the project. A.R.S. supervised the project. P.Z. and X.S. designed and performed experiments. C.C., K.i.W., and Z.L. assisted with experiments. S.S. and R.L. provided patient biopsy samples. F.H. and M.K. provided STAM and *MUP-uPA* mouse samples. J.L.W., M.K., and R.L. provided critique. P.Z., X.S., and A.R.S. wrote the manuscript.

Competing interests: A.R.S. and P.Z. are named inventors of a patent application related to the use of AMPK and caspase-6 as therapeutic targets for NASH. J.L.W. is a founding member of Oxitope. M.K. and A.R.S. are founders of Elgia Therapeutics. Other authors declare no competing interests.

Data availability: All data are available in the main text or supplementary materials.

SUPPLEMENTARY MATERIALS

science.sciencemag.org/content/367/6478/652/suppl/DC1

Materials and Methods

Figs. S1 to S10

Reference (41)

homeostasis, maintaining equilibrium between hepatocyte loss and replacement (3). However, pathological conditions such as viral infection, alcoholic or nonalcoholic steatohepatitis, and physical injury lead to extensive hepatocyte apoptosis and liver damage (4), which cause progressive fibrosis and cirrhosis (1, 5). Improving liver damage and preventing fibrosis are major goals of NASH therapy (2). Moreover, liver cell death is a major contributor to the pathogenesis of hepatocellular carcinoma (2). Therefore, understanding the molecular mechanisms that control hepatocellular death may lead to new treatments for liver diseases.

Adenosine monophosphate (AMP)-activated protein kinase (AMPK) is a key metabolic regulator that senses energy status and controls energy expenditure and storage (6). AMPK is allosterically activated by AMP and repressed by adenosine triphosphate (ATP) (6). Its activity is increased during undernutrition (7) and decreased during obesity (8, 9) and hyperglycemia (9) and by inhibitory phosphorylation driven by hyperinsulinemia and inflammation (10–12). Although activation of hepatic AMPK attenuates high-fat diet (HFD)-induced nonalcoholic fatty liver (NAFL), reducing AMPK activity does not cause or further worsen it (13). Whether the pathogenic repression of AMPK activity in obesity contributes to the occurrence of NASH and NASH-associated liver damage remains unknown.

Caspases are related aspartic-serine proteases that regulate inflammation and cell death. Apoptotic caspases are classified as “initiator,” such as caspase-8 and -9, or “executioner,” including caspase-3, -6, and -7 (14). Apoptotic cell death occurs through extrinsic and intrinsic pathways (15). The extrinsic pathway is driven by extracellular death receptor ligands, such as the tumor necrosis factor (TNF) superfamily and Fas ligand, and mediated by caspase-8. The intrinsic pathway is triggered by intracellular stress-induced cytochrome c release from mitochondria, leading to activation of the Apaf1-caspase-9 apoptosome. Both pathways converge in cleavage and activation of caspase-3 and -7 to execute programmed cell death (15). Although classified as an executioner, the mechanisms of activation and cleavage and the function of caspase-6 remain uncertain (14). We found that caspase-6 functions in steatosis-induced hepatocyte death and integrates signals from both inflammation and energy metabolism through direct phosphorylation by AMPK. Steatosis-induced decline in AMPK-catalyzed phosphorylation permits caspase-6 activation, leading to hepatocyte death. This link to obesity suggests that the AMPK-caspase-6 axis has a key role in NASH and might represent a new therapy.

Liver-specific AMPK knockout exaggerates liver damage in NASH

Hepatic AMPK activity is suppressed in diet-induced NAFL (9, 13). Although AMPK activation attenuates steatosis, loss of AMPK does not induce steatosis (13). Moreover, the role of AMPK in the pathogenesis of NASH remains uncertain. We generated liver-specific AMPK α 1/ α 2 (*Prkaa1/Prkaa2*) double-knockout (LAKO) mice that are devoid of hepatocyte expression of AMPK α 1 and - α 2, the catalytic subunits of AMPK (Fig. 1A). Liver-specific AMPK ablation did not affect body weight, liver weight, or triglycerides (TGs) in mice fed normal chow diet (ND) (fig. S1, A to C). ND-fed LAKO mice had normal serum alanine

aminotransferase (ALT), aspartate aminotransferase (AST), and alkaline phosphatase (ALP) activities and liver morphology (fig. S1, D to G).

We fed Flox and LAKO mice with a choline-deficient HFD (CD-HFD) to rapidly induce hepatic steatosis, liver damage, and fibrosis, which are characteristics of NASH (16). CD-HFD decreased AMPK Thr¹⁷² phosphorylation in livers of C57BL/6J mice, indicating repression of AMPK activity (Fig. 1B). LAKO mice were identical to Flox mice with respect to body weight, liver weight, or hepatic TGs (Fig. 1, C to E). However, a significant increase of serum ALT, AST, and ALP activities suggested exaggerated liver damage in CD-HFD-fed LAKO mice (Fig. 1, F to H). Increased liver terminal deoxynucleotidyl transferase-mediated deoxyuridine triphosphate nick end labeling (TUNEL) staining demonstrated that knockout of AMPK substantially increased the number of apoptotic cells, without affecting necroptotic cells identified by staining with phosphorylated mixed lineage kinase domain-like protein (phospho-MLKL) (Fig. 1, I and J). LAKO mice showed no changes in liver macrophage infiltration, as evidenced by similar macrophage marker F4/80 staining in Flox and LAKO mice (Fig. 1K). Nonetheless, hepatic fibrosis as measured with Sirius red staining and abundance of hydroxyproline was increased in LAKO mice, correlating with enhanced scarring from exaggerated liver damage (Fig. 1, K to M). LAKO did not affect the expression of the macrophage marker adhesion G protein-coupled receptor E1 (*Adgre1*, F4/80), the chemotactic cytokine C-C motif chemokine ligand 2 (*Ccl2*) and its receptor *Ccr2*, or pro-inflammatory cytokines tumor necrosis factor- α (*TNFA*) and interleukin-1 β (*Il1b*) (Fig. 1N). Although LAKO increased cell death and liver damage, the expression of cell death mediators caspase-3 (*Casp3*), *Casp8*, receptor-interacting serine/threonine protein kinase 1 (*Ripk1*), and *Ripk3* was not affected (Fig. 1O). Consistent with increased fibrosis, LAKO increased the expression of the fibrosis marker gene actin $\alpha 2$ (*Acta2*), collagen genes collagen type I $\alpha 1$ (*Col1a1*) and *Col3a1*, as well as hepatic stellate cell (HSC)-activating growth factor platelet-derived growth factor subunit B (*Pdgfb*) (Fig. 1P). LAKO mice showed no differences in the expression of transforming growth factor- β (*Tgfb*), the major macrophage-derived fibrogenic cytokine, which is consistent with similar macrophage infiltration in Flox and LAKO mice. Like-wise, LAKO mice showed no difference in growth factor *Pdgfa* and receptor *Pdgfra* expression or matrix remodeling genes tissue inhibitor matrix metalloproteinase 1 (*Timp1*) and discoidin domain receptor tyrosine kinase 2 (*Ddr2*) (Fig. 1P).

We also fed mice with the Amylin (AMLN) diet, which is used to mimic human NASH in preclinical studies (2, 17). AMLN also repressed AMPK activation in C57BL/6J mice (fig. S2A). LAKO had no effect on body weight, liver weight, liver-to-body weight ratio, hepatic TG, fasting glucose, glucose tolerance, or insulin resistance (fig. S2, B to H). LAKO did not affect the expression of *Adgre1*, gluconeogenic genes glucose-6-phosphatase catalytic subunit (*G6pc*) and phosphoenolpyruvate carboxykinase 1 (*Pck1*), lipogenic genes sterol regulatory element binding transcription factor 1 (*Srebf1*) and fatty acid synthase (*Fasn*), or mitochondria and lipid oxidation regulation genes peroxisome proliferator activated receptor γ coactivator 1 α (*Ppargc1a*) and carnitine palmitoyltransferase 1a (*Cpt1a*) (fig. S2, I to L) in AMLN-fed mice. However, LAKO significantly increased serum ALT, AST, and ALP activities, suggesting enhanced liver damage (fig. S2, M to O). LAKO mice had increased numbers of apoptotic liver cells (fig. S2, P and Q). Furthermore, exaggerated liver damage in

LAKO mice led to increased fibrosis (fig. S2, R to T). Similar to the results from CD-HFD-fed mice, LAKO increased the expression of fibrosis markers *Acta2*, *Coll1a1*, and *Col3a1* and fibrogenic growth factors *Pdgfa* and *Pdgfb*, with no effect on *Tgfb*, *Timp1*, *Pdgfra*, or *Ddr2* in AMLN-fed mice (fig. S2U). Thus, although LAKO did not further exaggerate steatosis or inflammation during NASH, hepatocellular death and fibrosis were enhanced.

AMPK deficiency increases caspase-6 activation to promote liver damage in NASH

To investigate the mechanism of exacerbated liver damage in NASH, we focused on proapoptotic caspases because necroptosis was not affected by LAKO. Cleavage of procaspase-6 and caspase-6 activity were increased in livers of LAKO mice on both CD-HFD (Fig. 2, A and B) and AMLN diets (fig. S3A). *Casp6* mRNA was not regulated by either diet (fig. S3B). LAKO significantly increased active caspase-6 (aCasp6) in livers of mice on CD-HFD (Fig. 2, C and D) or AMLN diet (fig. S3, C and D). Costaining of TUNEL and aCasp6 revealed TUNEL-stained nuclei located within cells with aCasp6 (Fig. 2E), correlating caspase-6 activation with hepatocellular death in NASH.

We examined the temporal relationship of caspase-6 activation and NASH development. Symptoms of NASH were apparent by 3 weeks of CD-HFD feeding, as evidenced by development of steatosis; TUNEL staining; and increased activities of ALT, AST, and ALP in serum. After 6 weeks, the mice developed extensive steatosis and substantial TUNEL staining, indicating well-established NASH (fig. S4, A to E). After 3 weeks of CD-HFD to develop NASH, Flox and LAKO mice were intravenously injected with control or caspase-6 small interfering RNA (siRNA) for 3 weeks during continuous CD-HFD (fig. S5A). Caspase-6 siRNA reduced hepatic *Casp6* mRNA by more than 80%. LAKO did not affect *Casp6* expression (fig. S5B). Caspase-6 depletion did not affect body or liver weight in CD-HFD-fed mice of either genotype (fig. S5, C and D). However, caspase-6 depletion reduced the number of apoptotic hepatocytes and serum ALT activity in both Flox and LAKO mice to a similar extent (Fig. 2, F to H). Depletion of caspase-6 significantly attenuated fibrosis in Flox and LAKO mice and nullified the deleterious effects of LAKO (fig. S5, E to G).

Caspase-6 is activated in mouse and human NASH

Because depleting caspase-6 attenuated liver damage in CD-HFD-induced NASH, we examined whether the activation of caspase-6 might occur in other NASH models, including HFD-fed streptozotocin-administered neonatal mice (18), HFD-fed major urinary protein-urokinase-type plasminogen activator (*MUP-uPA*) transgenic mice (19), or even human NASH. Caspase-6 was activated in livers of all mouse NASH models but not in healthy livers (Fig. 3A). The presence of NASH was validated with hematoxylin and eosin (H&E) staining (fig. S6A). To determine whether caspase-6 is activated in human NASH, we blindly assessed aCasp6 in liver sections of NASH patients, in whom liver status had been diagnosed. Caspase-6 was activated in livers from patients with NASH and cirrhosis (Fig. 3, B to D). Active caspase-6 significantly increased with Kleiner fibrosis score and positively correlated with severity of NASH (Fig. 3, B and C). Furthermore, whereas sections from normal livers had almost no active caspase-6 staining, the degree of active caspase-6 was

increased in cirrhosis (Fig. 3D). Moreover, whole-section scanning showed that both active caspase-6 and TUNEL staining were located within the cirrhotic nodule, indicating that caspase-6 might activate apoptosis of hepatocytes in human cirrhosis (Fig. 3E).

An AMPK agonist and a caspase-6 inhibitor therapeutically improve liver damage

To test the potential of AMPK as a therapeutic target, we fed C57BL/6J mice with CD-HFD for 6 weeks to establish NASH and then intraperitoneally injected mice with vehicle or AMPK agonist (A-769662) for 2 weeks while continuing CD-HFD (fig. S7A). In mice, AMPK β 1 is expressed in liver but not skeletal muscle (20). Thus, as an AMPK β 1 agonist, A-769662 activates AMPK in liver but not skeletal muscle. A previous study showed that injection of 30 mg/kg A-769662 twice per day for 7 days reduced hepatic TGs in C57BL/6J mice fed 45% HFD (13). In our study, injection of 25 mg/kg A-769662 once per day for 2 weeks in CD-HFD-fed mice had no effect on body weight, liver weight, or hepatic TG (fig. S7, B to D) but significantly reduced the number of apoptotic cells (Fig. 4, A and B, and fig. S7E) and improved liver damage (Fig. 4, C to E). A-769662 injection did not decrease the number of apoptotic cells nor reduce serum ALT activity in LAKO mice, indicating that A-769662 specifically targeted AMPK in hepatocytes to improve liver damage (fig. S7, F to H). A-769662 attenuated hepatic fibrosis (Fig. 4, F to H) and significantly reduced the expression of fibrotic genes *Colla1*, *Col3a1*, *Pdgfa*, *Pdgfb*, and *Pdgfra*, without effect on *Tgfb*, *Ddr2*, or inflammation marker genes *Adgre1* or *Ccl2* (Fig. 4I and fig. S7I).

To examine whether caspase-6 inhibition might also improve liver damage and decrease the effects of AMPK deficiency, we fed Flox and LAKO mice with CD-HFD for 6 weeks to establish NASH and then intraperitoneally injected vehicle or the caspase-6 inhibitor Z-VEID-FMK (VEID) for 2 weeks while continuing CD-HFD (fig. S8A). VEID did not affect body or liver weight (fig. S8, B and C) but significantly reduced the number of apoptotic hepatocytes and decreased serum ALT activity in both Flox and LAKO mice (Fig. 4, J to L, and fig. S8D). VEID abrogated the difference in liver damage between Flox and LAKO mice. VEID reduced liver fibrosis in both Flox and LAKO mice and abolished the effect of AMPK deficiency (fig. S8, E to G), further suggesting that AMPK–caspase-6 axis critically controls liver damage.

AMPK phosphorylates procaspase-6 to inhibit its cleavage and activation

To explore the regulation of caspase-6, we treated primary hepatocytes with TNF α and palmitic acid (PA) to mimic inflammation and lipotoxicity-induced hepatocellular death. Both induced caspase-6 activation (fig. S9A). To determine whether the AMPK agonist directly inhibited procaspase-6 cleavage in a cell-autonomous manner, we treated primary hepatocytes or HepG2 cells with A-769662 and then, to induce procaspase-6 cleavage, with TNF α and cycloheximide (CHX). In both cells, A-769662 significantly inhibited procaspase-6 cleavage (Fig. 5A and fig. S9B). The induction of caspase-6 activity by PA was also inhibited in cells pretreated with A-769662 (Fig. 5B). In silico analysis revealed one AMPK substrate motif site on procaspase-6 Ser²⁵⁷ (Fig. 5C) (21). Procaspase-6 Ser²⁵⁷ is phosphorylated by AMPK-related protein kinase 5 (ARK5) in colorectal adenocarcinoma

cells (22). Phosphorylation of Ser²⁵⁷ represses procaspase-6 cleavage and activation (23). Both recombinant AMPK α 1 and AMPK α 2 directly phosphorylated procaspase-6 at Ser²⁵⁷ in vitro (Fig. 5D and fig. S9C). The Ser²⁵⁷ site and the surrounding sequence in caspase-6 are conserved across species (Fig. 5E). We overexpressed wild-type procaspase-6, or its S257A non-phospho-mimetic mutant, or S257D/S257E phospho-mimetic mutants in human embryonic kidney (HEK) 293T cells and subsequently treated the cells with low doses of TNF α and CHX to induce procaspase-6 cleavage. The S257A mutant was more sensitive to cleavage, whereas both the S257D and S257E mutants were completely resistant (Fig. 5F). Moreover, A-769662 significantly increased procaspase-6 Ser²⁵⁷ phosphorylation (Fig. 5G) and decreased caspase-6 activity in vivo (Fig. 5H). AMPK activation decreased aCasp6 in CD-HFD-induced NASH (Fig. 5, I and J). Analysis of liver lysates from CD-HFD-fed Flox and LAKO mice administered vehicle or A-769662 revealed that A-769662 significantly increased procaspase-6 phosphorylation and decreased procaspase-6 cleavage in Flox but not in LAKO mice (fig. S9,D and E). AMPK deficiency itself decreased procaspase-6 phosphorylation and increased procaspase-6 cleavage (fig. S9, D and E). Moreover, CD-HFD decreased procaspase-6 phosphorylation, correlating with the increased procaspase-6 cleavage and decreased AMPK phosphorylation (Figs. 1B and 5K and fig. S9F).

Caspase-6 mediates a feedforward loop to sustain the caspase cascade

To understand how caspase-6 controls the pathogenesis of NASH, we investigated its role in the apoptotic pathways. Depletion of caspase-6 in HepG2 cells significantly increased cell viability after 20 hours of treatment with TNF α and CHX (fig. S10A). An in vitro cleavage assay showed that procaspase-6 was directly cleaved by caspase-3 and -7 but not caspase-8 or -9 (Fig. 6A). Pretreatment with a caspase-3 and -7 inhibitor largely attenuated procaspase-6 cleavage caused by TNF α and CHX (Fig. 6B). These data suggest that caspase-6 is activated by executioner caspases but not initiators.

We searched for a relevant substrate and found that active caspase-6 cleaved purified Bcl2 family protein Bid (BH3 interacting-domain death agonist) but not Bax (Bcl2-associated X) in vitro (Fig. 6C). Both of these proteins contribute to cytochrome c release and subsequent cell damage (24, 25). Active caspase-6 cleaves Bid to generate two cleaved peptide fragments (Fig. 6D), one with a size similar to that of caspase-8-cleaved Bid (26) and another that was smaller. N-terminal sequencing showed that active caspase-6 cleaved Bid at both Asp⁵⁹ and Asp⁷⁵ (Fig. 6, E and F); both cleavages activate Bid to induce cytochrome c release (26, 27). Because cleavage of Bid induces mitochondrial cytochrome c release into the cytoplasm (24, 25), we fractionated liver from vehicle or VEID-treated Flox and LAKO mice to isolate cytosolic (Cyto) and mitochondrial (Mito) fractions. Cytosolic cytochrome c was increased in LAKO mice. VEID treatment decreased cytosolic cytochrome c in both Flox and LAKO mice and completely abrogated the effect of LAKO (Fig. 6G).

We wondered whether caspase-6 might mediate a feedforward loop of the caspase cascade because it is cleaved by the executioner caspases-3 and -7 and in turn induces cytochrome c release. HepG2 cells were transfected with scrambled control or caspase-6 siRNA and treated with vehicle or CHX plus TNF α for 2 hours to induce caspase activation. Two hours after the medium change, amounts of cleaved caspase-9, -3, and -7 were similar in control

or caspase-6–depleted cells. However, after 5 hours, caspase-6–depleted cells had significantly less cleaved caspase-9, -3, and -7 (Fig. 6H and fig. S10B). Thus, activation of the caspase cascade appears to diminish faster in caspase-6–depleted cells. Inhibition of caspase-6 with VEID also led to a substantial decrease of cleaved caspase-3 and -7 in primary hepatocytes (fig. S10C). Caspase-6 may mediate a feedforward loop to sustain activation of the caspase cascade, in which cytochrome c can potentiate the activation of the upstream caspases, and this sustained activation may be necessary for extensive apoptosis (Fig. 6I). This process is only activated under conditions of excess energy accumulation due to reduced AMPK activity.

Discussion

Overnutrition-induced hepatic steatosis and inflammation lead to liver damage in NASH (2). We describe here an AMPK–caspase-6 axis that regulates hepatocellular apoptosis and may shed new light on the “two-hit” or “multiple-hit” hypothesis of NASH. Inflammation in NAFL disease (NAFLD) leads to caspase-6 activation by the increased activity of upstream executioners caspase-3 and -7. Active caspase-6 in turn cleaves Bid to increase mitochondrial cytochrome c release in a feedforward loop, in which activation of upstream caspases is persistent, so that the apoptotic caspase cascade is sustained in hepatocytes. However, in the metabolically healthy liver, AMPK activity is maintained to allow phosphorylation of procaspase-6, which inhibits its activation, thus preventing this feedforward loop (Fig. 6I and fig. S10D). When AMPK activity is reduced through overnutrition, hyperglycemia, hyperinsulinemia, and inflammation in obesity, diabetes, and NAFL, caspase-6 is derepressed, leading to activation of the feedforward loop, priming hepatocytes for caspase-mediated apoptosis (fig. S10D) (28). AMPK inhibition may thus serve as a point of convergence by which overnutrition, steatosis, hyperinsulinemia, and inflammation contribute to liver damage. If so, pharmaceutical interventions that specifically activate AMPK or block caspase-6 in livers may represent approaches to treat NASH.

Caspase-2 triggers de novo lipogenesis and steatosis during NAFL (19). By contrast, caspase-6 does not contribute to the development of steatosis but specifically mediates NASH-associated liver damage. Although knockout of caspase-3 and -8 also protects against hepatocyte apoptosis (29, 30), global knockout of caspase-8 is embryonically lethal, whereas caspase-3 whole-body knockout leads to multiple developmental defects (31, 32). By contrast, caspase-6–deficient mice exhibit no developmental defects (14). It is possible that specifically targeting caspase-6 could be an effective therapeutic strategy with fewer side effects.

In AMLN- and CD-HFD–fed mice, both of which exhibit characteristics of human NASH, LAKO exaggerates liver damage without affecting steatosis and inflammation. Exacerbation of liver damage leads to increased scarring and fibrosis. Two weeks treatment with both AMPK activator and caspase-6 inhibitor substantially reduced hepatocellular death and hepatic fibrosis. Activation of AMPK inhibits proliferation of HSCs (33). Thus, the effects of the AMPK activator reported here on hepatic fibrosis could be attributed to both reduction of liver damage and inhibition of HSCs.

We measured caspase-6 activity with the VEID-pNA substrate, and Z-VEID-FMK was used as a caspase-6 inhibitor. Although VEID is a preferred substrate of caspase-6, it cross-reacts to a lesser extent with caspase-3 (34, 35). To ensure specificity, we used multiple methodologies to determine activation of caspase-6, including Western blot and immunofluorescent staining of aCasp6. We also used siRNA to specifically deplete caspase-6, resulting in attenuation of liver damage in NASH. Taken together, our data support the conclusion that caspase-6 is activated and participates in the pathogenesis of liver damage in NASH. Moreover, depletion of caspase-6 abrogated the exaggerated liver damage in LAKO mice, indicating that the AMPK–caspase-6 axis regulates liver damage.

A previous study showed that inhibition of caspase-3 and –7 attenuates Bid cleavage, suggesting the existence of a feedforward loop that acts downstream of the executioner caspases (36). We elaborated the role of caspase-6 in sustaining activation of the caspase cascade in this feedforward loop. A previous study demonstrated that caspase-6 cleaves lamin A to induce nuclear and chromatin condensation in apoptosis (37). Although we observed some nuclear localization of active caspase-6 in our human and mouse NASH samples, most of active caspase-6 appeared to locate within the cytoplasm, suggesting that cleavage of Bid could be a dominant function of caspase-6. However, because caspase-6 does not participate in the initiating activation of the caspase cascade, it may play a role in mediating apoptosis only in chronic diseases. Caspase-6 has been proposed as an important target in Alzheimer's disease (38, 39), which is also characterized by reduced AMPK activity (40). Thus, the AMPK–caspase-6 axis might have a role in other chronic inflammatory pathogenic processes.

Supplementary Material

Refer to Web version on PubMed Central for supplementary material.

ACKNOWLEDGMENTS

We thank S. J. Morrison at the University of Texas Southwestern and K. Inoki at the University of Michigan for sharing AMPK α 1 and α 2 floxed mice and University of California, San Diego (UCSD) histology core for histology study.

Funding: This work was supported by NIH P30DK063491, R01DK076906, and R01DK117551 to A.R.S.; NIH K99HL143277 to P.Z.; AHA 18POST34060088 to X.S.; NIH P01HL088093 to J.L.W.; NIH R01DK120714 to M.K.; NIH P42ES010337, UL1TR001442, R01DK106419, and P30DK120515 and U.S. Department of Defense (DOD) CA170674P2 to R.L.; and National Institute of Neurological Disorders and Stroke P30NS047101 to the UCSD microscopy core. F.H. was supported by the Eli Lilly LIFA program.

REFERENCES AND NOTES

1. Hernandez-Gea V, Friedman SL, Annu. Rev. Pathol 6, 425–456 (2011). [PubMed: 21073339]
2. Friedman SL, Neuschwander-Tetri BA, Rinella M, Sanyal AJ, Nat. Med 24, 908–922 (2018). [PubMed: 29967350]
3. Michalopoulos GK, DeFrances M, Adv. Biochem. Eng. Biotechnol 93, 101–134 (2005). [PubMed: 15791946]
4. Guicciardi ME, Gores GJ, Gut 54, 1024–1033 (2005). [PubMed: 15951554]
5. Luedde T, Kaplowitz N, Schwabe RF, Gastroenterology 147, 765–783.e4 (2014). [PubMed: 25046161]

6. Hardie DG, Genes Dev. 25, 1895–1908 (2011). [PubMed: 21937710]
7. Hardie DG, Ross FA, Hawley SA, Nat. Rev. Mol. Cell Biol 13, 251–262 (2012). [PubMed: 22436748]
8. Martin TL et al., J. Biol. Chem 281, 18933–18941 (2006). [PubMed: 16687413]
9. Viollet B. et al., Crit. Rev. Biochem. Mol. Biol 45, 276–295 (2010). [PubMed: 20522000]
10. Valentine RJ, Coughlan KA, Ruderman NB, Saha AK, Arch. Biochem. Biophys 562, 62–69 (2014). [PubMed: 25172224]
11. Zhao P. et al., Cell 172, 731–743.e12 (2018). [PubMed: 29425491]
12. Steinberg GR et al., Cell Metab. 4, 465–474 (2006). [PubMed: 17141630]
13. Boudaba N. et al., EBioMedicine 28, 194–209 (2018). [PubMed: 29343420]
14. McIlwain DR, Berger T, Mak TW, Cold Spring Harb. Perspect. Biol 5, a008656 (2013). [PubMed: 23545416]
15. Budihardjo I, Oliver H, Lutter M, Luo X, Wang X, Annu. Rev. Cell Dev. Biol 15, 269–290 (1999). [PubMed: 10611963]
16. Matsumoto M. et al., Int. J. Exp. Pathol 94, 93–103 (2013). [PubMed: 23305254]
17. Clapper JR et al., Am. J. Physiol. Gastrointest. Liver Physiol 305, G483–G495 (2013). [PubMed: 23886860]
18. Fujii M. et al., Med. Mol. Morphol 46, 141–152 (2013). [PubMed: 23430399]
19. Kim JY et al., Cell 175, 133–145.e15 (2018). [PubMed: 30220454]
20. Cokorinos EC et al., Cell Metab. 25, 1147–1159.e10 (2017). [PubMed: 28467931]
21. Wu D. et al., Nature 559, 637–641 (2018). [PubMed: 30022161]
22. Suzuki A. et al., Oncogene 23, 7067–7075 (2004). [PubMed: 15273717]
23. Velázquez-Delgado EM, Hardy JA, Structure 20, 742–751 (2012). [PubMed: 22483120]
24. Eskes R, Desagher S, Antonsson B, Martinou JC, Mol. Cell. Biol 20, 929–935 (2000). [PubMed: 10629050]
25. Wei MC et al., Genes Dev. 14, 2060–2071 (2000). [PubMed: 10950869]
26. Li H, Zhu H, Xu CJ, Yuan J, Cell 94, 491–501 (1998). [PubMed: 9727492]
27. Sutton VR et al., J. Exp. Med 192, 1403–1414 (2000). [PubMed: 11085743]
28. Drew L, Nature 550, S102–S103 (2017). [PubMed: 29019968]
29. Hatting M. et al., Hepatology 57, 2189–2201 (2013). [PubMed: 23339067]
30. Thapaliya S. et al., Dig. Dis. Sci 59, 1197–1206 (2014). [PubMed: 24795036]
31. Kaiser WJ et al., Nature 471, 368–372 (2011). [PubMed: 21368762]
32. Kuida K. et al., Nature 384, 368–372 (1996). [PubMed: 8934524]
33. da Silva Morais A. et al., Clin. Sci. (Lond.) 118, 411–420 (2009). [PubMed: 19852755]
34. Ehrnhoefer DE et al., PLOS ONE 6, e27680 (2011). [PubMed: 22140457]
35. Heise CE et al., PLOS ONE 7, e50864 (2012). [PubMed: 23227217]
36. Shelton SN, Shawgo ME, Robertson JD, J. Biol. Chem 284, 11247–11255 (2009). [PubMed: 19233849]
37. Ruchaud S. et al., EMBO J. 21, 1967–1977 (2002). [PubMed: 11953316]
38. LeBlanc AC, Eur. J. Neurosci 37, 2005–2018 (2013). [PubMed: 23773070]
39. Wang XJ, Cao Q, Zhang Y, Su XD, Annu. Rev. Pharmacol. Toxicol 55, 553–572 (2015). [PubMed: 25340928]
40. Salminen A, Kaarniranta K, Haapasalo A, Soinen H, Hiltunen M, J. Neurochem 118, 460–474 (2011). [PubMed: 21623793]

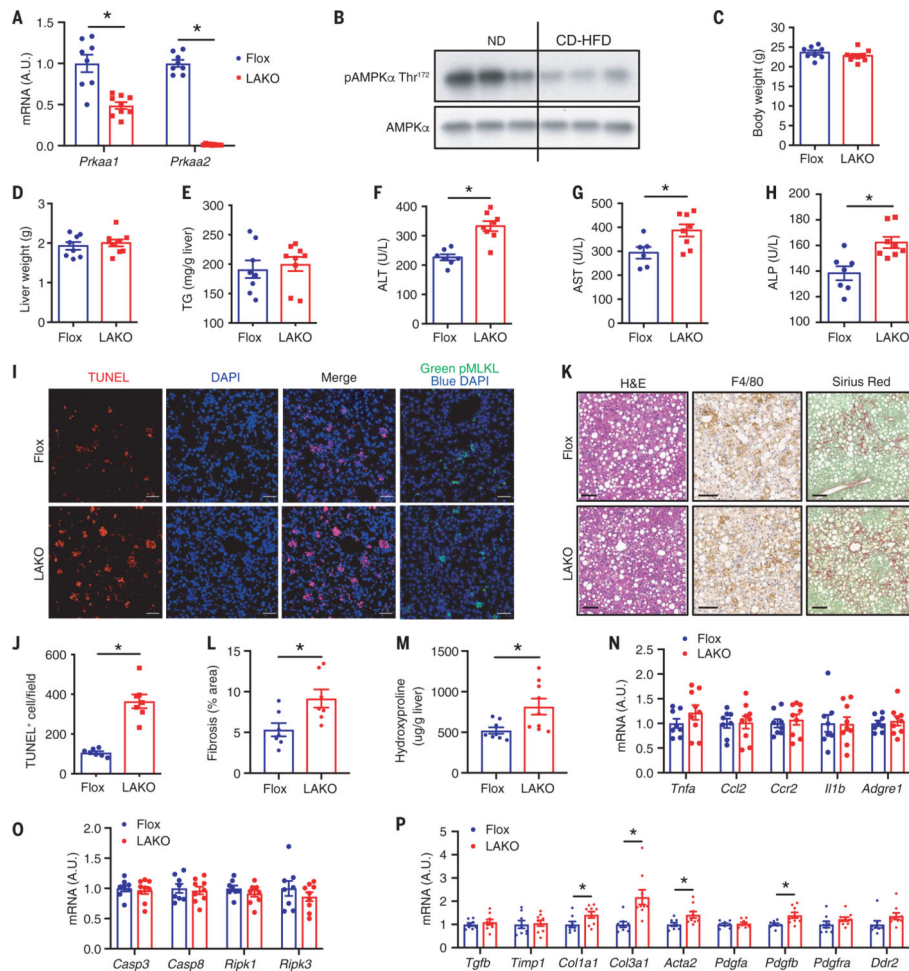


Fig. 1. Liver-specific AMPK knockout exacerbates liver damage in NASH.

(A) Expression of *Prkaa1* and *Prkaa2* in liver; $n = 8$ to 9 mice. A.U., arbitrary units. (B) Immunoblot of liver lysate from ND or CD-HFD-fed mice; $n = 3$ mice. (C to P) Flox and LAKO mice fed CD-HFD for 11 weeks. (C) Body weight. (D) liver weight. (E) Liver TG. [(F) to (H)] Serum ALT (F), AST (G), ALP (H); $n = 8$ to 9 mice. (I) Liver sections stained TUNEL (red) and 4',6-diamidino-2-phenylindole (DAPI) (blue) or pMLKL (Green). Scale bar, 50 μ m. (J) Quantification of TUNEL-positive nuclei per field in (I); $n = 7$ mice. (K) H&E, F4/80, and Sirius red staining of liver sections. Scale bar, 100 μ m; $n = 7$ mice. (L) Quantification of fibrosis area (percent of total area) shown in (K); $n = 7$ mice. (M) Liver hydroxyproline; $n = 8$ to 9 mice. (N) Expression of *TNFA*, *Ccl2*, *Ccr2*, *Il1b*, and *Adgre1* in liver; $n = 8$ to 9 mice. (O) Expression of *Casp3*, *Casp8*, *Ripk1*, and *Ripk3* in liver; $n = 8$ to 9 mice. (P) Expression of *Tgfb*, *Timp1*, *Col1a1*, *Col3a1*, *Acta2*, *Pdgfa*, *Pdgfb*, *Pdgfra*, and *Ddr2* in liver; $n = 8$ to 9 mice. Mean \pm SEM; * $P < 0.05$, Student's unpaired *t* test.

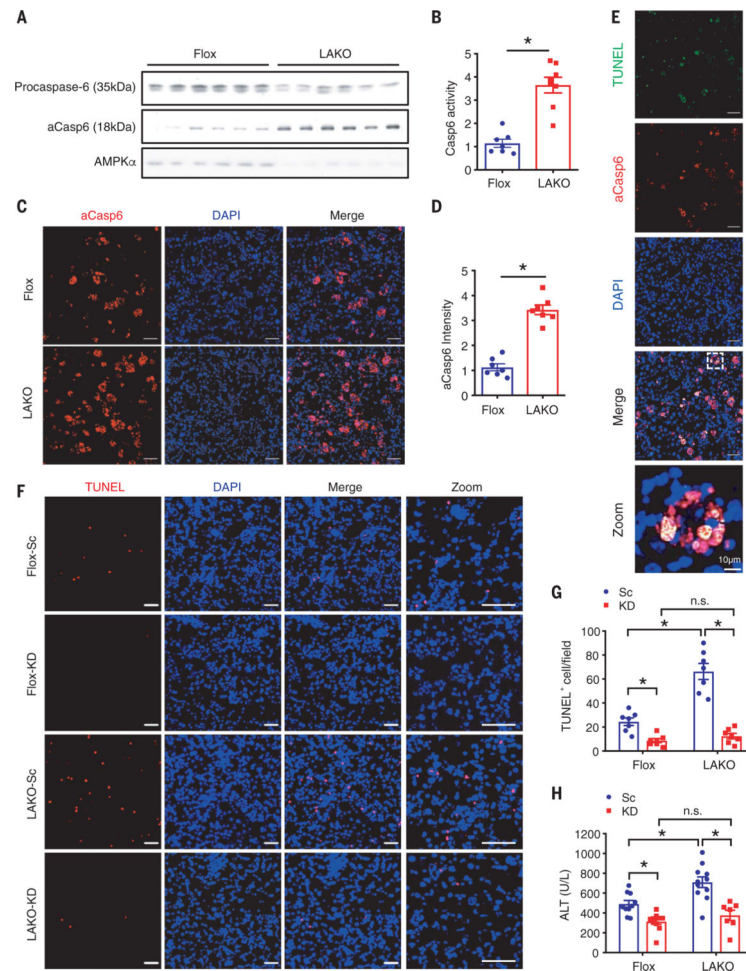


Fig. 2. AMPK deficiency increases caspase-6 cleavage to promote liver damage in NASH. (A to E) Flox and LAKO mice fed CD-HFD for 11 weeks. (A) Immunoblot analysis of liver lysate; $n = 6$ mice. (B) Casp6 activity in liver lysate; $n = 7$ to 8 mice. (C) Liver sections stained active Caspase-6 (aCasp6, red) and DAPI (blue). Scale bar, 50 μm . (D) Quantification of aCasp6 staining in (C); $n = 7$ mice. (E) Liver sections stained TUNEL (green), aCasp6 (red), and DAPI (blue). Scale bar, 50 μm . * $P < 0.05$, Student's unpaired t test. (F to H) Flox and LAKO mice fed with CD-HFD for 3 weeks, followed by intravenous injection of 1.5 mg/kg caspase-6 siRNA (KD) or scrambled RNA (Sc) twice per week for 3 weeks while fed continuous CD-HFD. (F) Liver sections stained TUNEL (red) and DAPI (blue). Scale bar, 50 μm . (G) Quantification of TUNEL-positive nuclei per field in (F); $n = 7$ mice. (H) Serum ALT; $n = 7$ to 10 mice. Mean \pm SEM; * $P < 0.05$, two-way analysis of variance (ANOVA).

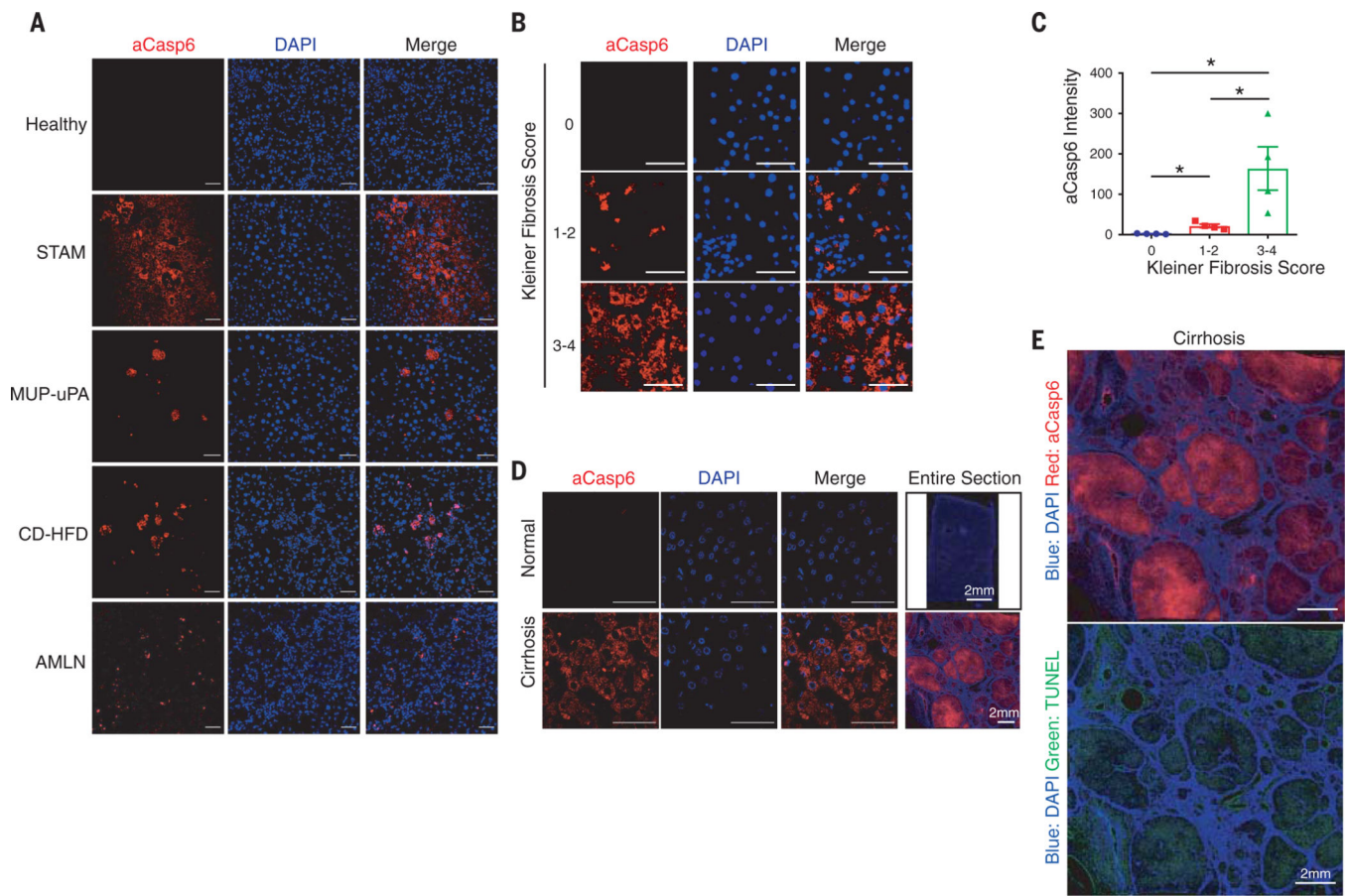


Fig. 3. Caspase-6 is activated in mouse and human NASH.

(A) Healthy model: 24-weeks-old male C57BL/6J mice fed ND. STAM-NASH model: male C57BL/6J mice were subcutaneously injected 200 μ g streptozotocin (STZ) within 48 hours after birth and fed HFD for 6 weeks starting at 4 weeks of age. *MUP-uPA*-NASH model: male *MUP-uPA* mice fed 60% HFD for 16 weeks. CD-HFD-NASH model: C57BL/6J mice were fed CD-HFD for 11 weeks. AMLN-NASH model: C57BL/6J mice fed AMLN diet for 30 weeks. Liver sections were stained with aCasp6 (red) and DAPI (blue). Scale bar, 50 μ m. (B) Human liver sections were classified blindly by liver pathologist and stained with aCasp6 (Kleiner fibrosis score 0, 1 to 2, and 3 to 4). Scale bar, 50 μ m. (C) Quantification of aCasp6 staining in (B), plotted against Kleiner fibrosis scores; $n = 4$ human subjects. (D) Human liver sections were stained aCasp6 to compare caspase-6 activation in healthy and cirrhotic donors. Scale bar, 50 μ m. (E) Scanning of human liver section stained aCasp6 (red), TUNEL (green), and DAPI. Scale bar, 2 mm. Mean \pm SEM; * $P < 0.05$, Student's unpaired t test.

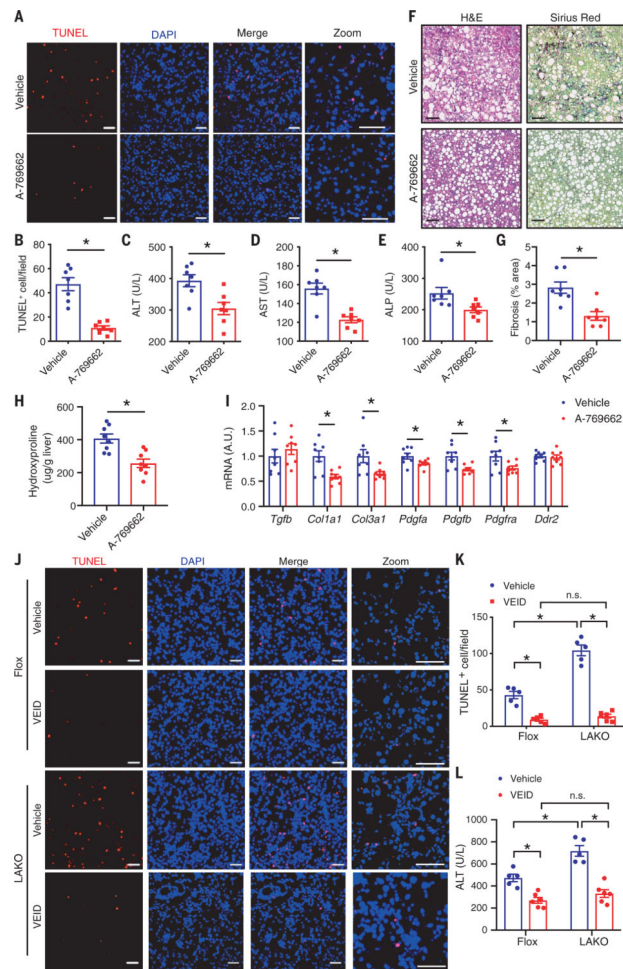


Fig. 4. Both an AMPK agonist and a caspase-6 inhibitor therapeutically improve liver damage. (A to I) C57BL/6J mice were fed CD-HFD for 6 weeks, followed by intraperitoneal injection of 25 mg/kg A-769662 or vehicle daily for 2 weeks while fed continuous CD-HFD. (A) Liver sections stained TUNEL (red) and DAPI (blue). Scale bar, 50 μ m. (B) Quantification of TUNEL-positive nuclei per field in (A); $n = 7$ mice. [(C) to (E)] Serum ALT (C), AST (D), and ALP (E); $n = 7$ mice. (F) H&E and Sirius red staining of liver sections. Scale bar, 100 μ m. (G) Quantification of liver fibrosis area (percent of total area) in (F); $n = 7$ mice. (H) Liver hydroxyproline; $n = 8$ mice. (I) Expression of *Tgfb*, *Timp1*, *Col1a1*, *Col3a1*, *Pdgfa*, *Pdgfb*, *Pdgfra*, and *Ddr2* in livers; $n = 8$ mice. * $P < 0.05$, Student's unpaired *t* test. (J to L) Flox and LAKO mice were fed CD-HFD for 6 weeks, followed by intraperitoneal injection of 5 mg/kg VEID or vehicle every other day for 2 weeks while continuously feeding. (J) Liver sections stained TUNEL (red) and DAPI (blue). Scale bar, 50 μ m. (K) Quantification of TUNEL-positive nuclei per field in (J); $n = 5$ to 6 mice. Mean \pm SEM; * $P < 0.05$, two-way ANOVA.

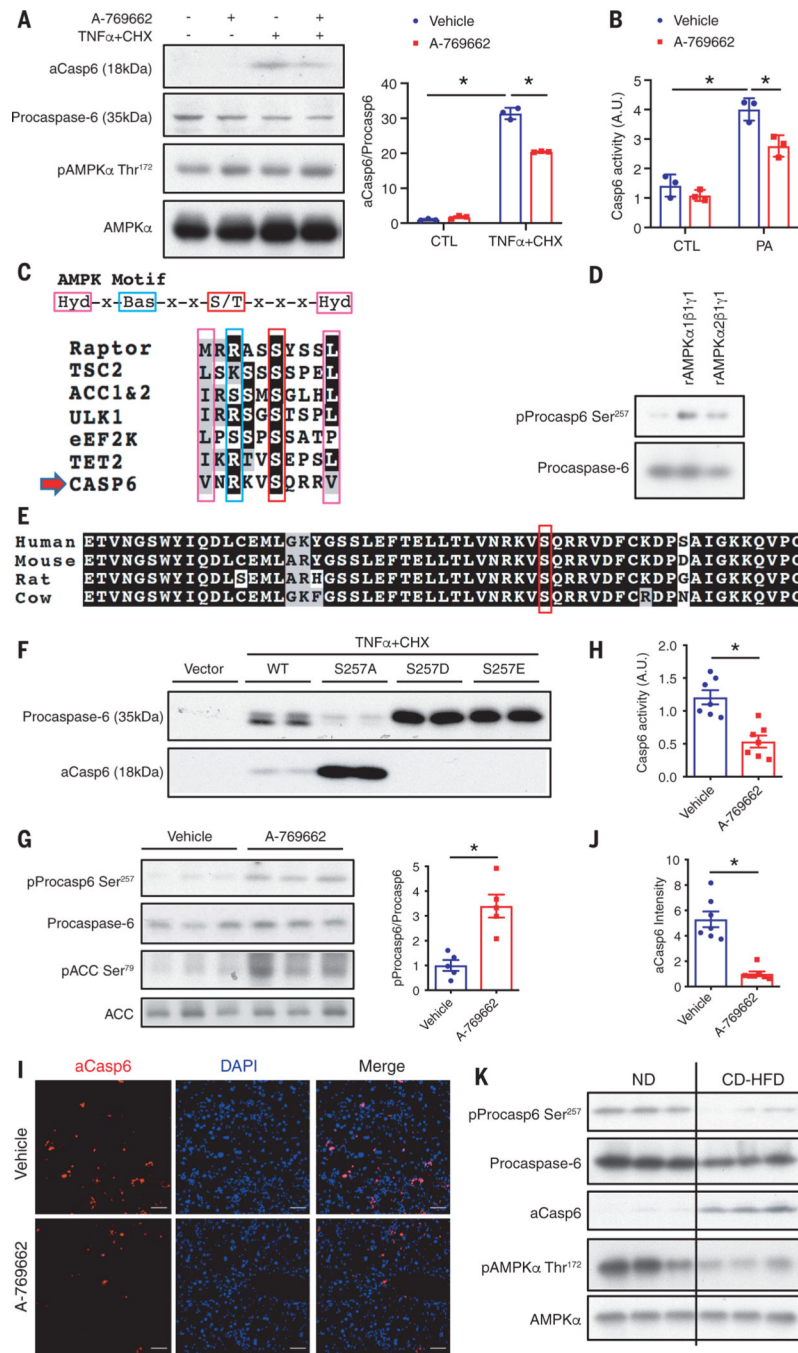


Fig. 5. AMPK phosphorylates caspase-6 to inhibit its cleavage and activation.

(A) Primary hepatocytes were pretreated with 40 μ M A-769662 for 1 hour then treated with 30 μ g/ml CHX and 50 ng/ml TNF α for 2 hours. Shown is immunoblot analysis of cell lysates; $n = 3$ independent experiments. Mean \pm SD; * $P < 0.05$, two-way ANOVA. (B) Primary hepatocytes were pretreated with 40 μ M A-769662 for 1 hour then treated with 250 μ M bovine serum albumin (BSA)-conjugated PA for 2 hours. Cell lysates were subject to caspase-6 activity assay. Mean \pm SD; * $P < 0.05$. (C) Caspase-6 Ser²⁵⁷ locates within AMPK substrate motif. (D) In vitro kinase assay using recombinant caspase-6 and recombinant

AMPK α 1 β 1 γ 1 or AMPK α 2 β 1 γ 1 active kinase. **(E)** Alignment of caspase-6 sequence. **(F)** HEK293T cells overexpressing caspase-6-myc wild type, S257A, S257D, or S257E mutant were treated with 10 μ g/ml CHX and 25 ng/ml TNF α for 2 hours. Shown is immunoblot analysis of cell lysates. (Single-letter abbreviations for the amino acid residues are as follows: A, Ala; D, Asp; E, Glu; S, Ser. In the mutants, other amino acids were substituted at certain locations; for example, S257A indicates that serine at position 257 was replaced by alanine.) **(G to J)** C57BL/6J mice were fed CD-HFD for 6 weeks, followed by intraperitoneal injection of 25 mg/kg A-769662 or vehicle daily for 2 weeks while fed continuous CD-HFD. Mice were euthanized 6 hours after the last injection. **(G)** Immunoblot analysis of liver lysates; $n = 5$ mice. **(H)** Liver lysates were subject to caspase-6 activity assay; $n = 7$ mice. **(I)** Liver sections stained with aCasp6 (red) and DAPI (blue). Scale bar, 50 μ m. **(J)** Quantification of aCasp6 staining per field in **(I)**; $n = 7$ mice. Mean \pm SEM; * $P < 0.05$, Student's unpaired t test. **(K)** Immunoblot analysis of liver lysates from C57BL/6J mice fed ND or CD-HFD. AMPK and pAMPK blots are the same as in Fig. 1B.

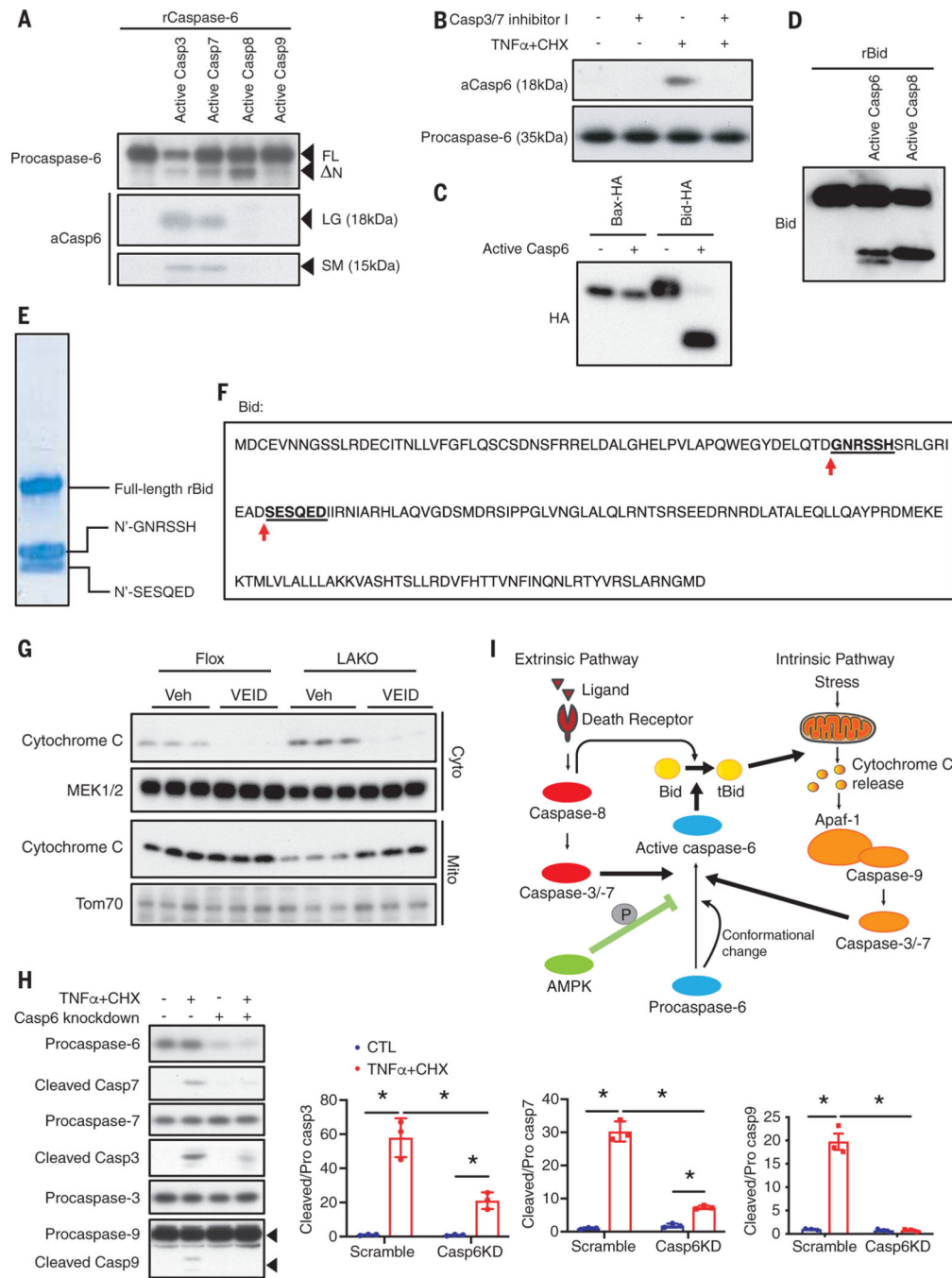


Fig. 6. Caspase-6 mediates a feedforward loop to sustain the caspase cascade.

(A) In vitro cleavage assay using recombinant procaspase-6 with active caspase-3, -7, -8, or -9. FL, full-length; N, n terminus deleted form; LG, large; SM, small. (B) Primary hepatocytes were pretreated with 10 μM caspase-3/7 inhibitor I for 1 hour then treated with 30 μg/ml CHX and 50 ng/ml TNFα for 2 hours. Immunoblot analysis of cell lysates. (C) In vitro cleavage assay using purified Bid-HA or Bax-HA expressed in HEK293T cells, and active caspase-6. (D) In vitro cleavage assay using recombinant Bid with active caspase-6 or -8. (E) In vitro cleavage assay using recombinant Bid with active caspase-6. Bands for

cleaved Bid were subject to Edman degradation. **(F)** Bid sequence and sites cleaved by active caspase-6. **(G)** Flox and LAKO mice were fed CD-HFD for 6 weeks, followed by intraperitoneal injection of 5 mg/kg VEID or vehicle every other day for 2 weeks while fed continuous CD-HFD. Livers were fractionated to separate cytosolic and mitochondrial extract for immunoblot analysis. **(H)** HepG2 cells transfected scrambled RNA or Caspase-6 siRNA were treated with vehicle or 30 $\mu\text{g/ml}$ CHX and 50 ng/ml TNF α for 2 hours. Medium was changed to remove treatment for 5 hours. Cell lysates were subject to immunoblot analysis; $n = 3$ independent experiments. Mean \pm SD; * $P < 0.05$, two-way ANOVA. **(I)** Proposed model for roles of AMPK–caspase-6 axis in apoptotic caspase cascade.